Supporting Information

Nitrogen defective and porous self-supporting structure carbon nitride for visible light hydrogen evolution

Jun Han [a], Fangzhou Wu [a], Zhongwei wang [c], Xiyu Chen [a], De Hu [a], Feng Yu [a], Yan Gao [c] [*], Bin Dai [a*], Wei Wang [a, b*]

a. School of Chemistry and Chemical Engineering, Shihezi University, Shihezi 832003, China

b. School of Chemical Engineering, Shandong Institute of Petroleum and Chemical Technology, Shandong 257061, China

c. College of Science, Shihezi University, Shihezi 832003, China

*Corresponding author: Wei Wang. E-mail: wangw@shzu.edu.cn

*Corresponding author: Bin Dai. E-mail: dbinly@126.com

*Corresponding author: Yan Gao. E-mail: gaoy@shzu.edu.cn

Fig.S1 SEM images of NP (a), TMCN (c), MP(c) and MCN (d).

Fig. S2 HRTEM images of PCN (a) and TMCN (b).

Fig.S3 Mapping and EDS images of PCN (a) and TMCN (b).

Fig. S4 Photo-responsive linear sweep voltammetry curves of PCN and TMCN.

Fig. S5. Photocatalytic H_2 production rates of MCN.

Tab.S1 BET specific surface area and pore volume.

Tab.S2 Atomic content of different elements in XPS spectrum.

Tab.S3 Peak integration area of different carbon state in C1s spectrum.

Tab.S4 Peak integration area of different carbon state in N1s spectrum.

Tab. S5 C/N atomic ratio in EA.

1.1. Characterizations

The morphologies of all samples were examined using high-resolution transmission electron microscopy (HRTEM, JEOL JEM-2010HR) and scanning electron microscopy (SEM, JEOL JSM-6490). The crystal structure was determined by collecting powder X-ray diffraction (XRD) patterns using a D8-Advance X-ray diffractometer with Cu Kα radiation (λ=0.15406 nm). The scanning rate was set at 10° min^{-1}, and the voltage and current were 40 kV and 40 mA, respectively. The chemical composition and the functional group information were explored by Fourier transform infrared spectroscopy (FT-IR) on a FT-IR spectrometer (Bruker Vertex 70V) and X-ray photoelectron spectroscopy (XPS) on a Thermo Scientific ESCALAB 250Xi with a standard Al Kα X-ray source. Electron paramagnetic resonance (EPR) measurements were conducted using a Bruker EMXplus-6/1 spectrometer at room temperature. Elemental analysis results were obtained using an Elementar UNICUBE analyzer. The specific surface area and pore volume were characterized using the Brunauer-Emmett-Teller (BET) nitrogen adsorption-desorption isotherm method on a Micromeritics APSP 2460 instrument. The optical response and band gaps of all samples were evaluated using ultraviolet-visible diffuse reflectance spectrum (UV-vis DRS) on a Shimadzu 2600U UV-vis spectrometer, with $BaSO_4$ base used as the reflection standard. The recombination rate of photogenerated electron-hole pairs was estimated by collecting the photoluminescence (PL) spectrum using a fluorescence spectrophotometer (HITACHI F700/F-7000/F-7100) with an excitation wavelength of 340 nm.

1.2. Photoelectrochemical measurement

Photoelectrochemical measurements were performed on an electrochemical workstation (CH760E), using platinum and Ag/AgCl as the counter electrode and reference electrode, respectively. The photoelectrode was prepared by the quantitative drop-coating method. Disperse 1 mg of photocatalyst in 0.75 mL of H_2O, then add 0.25 mL of ethyl alcohol and 25 µL of nafion to it, and then sonicate for 10 minutes. Take 150 µL of the suspension drop and spread it on indium tin oxide (ITO) coated glass (length $\times$ width = 2 cm $\times$ 1 cm) and dried in air. Na_2SO_4 solution (0.2 mol/L, pH = 7.0) was used as electrolyte solution. The external light source is provided by a 300 W xenon lamp equipped with a 420 nm filter.

1.3. DFT calculation

The Vienna ab initio simulation package (VASP) was used to perform spin-polarized DFT calculations with Perdew, Burke, and Ernzerhof (PBE) functionals. The projector augmented wave (PAW) method was used to calculate the interactions between ions and electrons. Long-range vander Waals (vdW) interactions were handled by the DFT-D3 method. During structural optimizations, the convergence criteria of total energy and minimum force were set to 10^{-5} eV and 0.02 eV/Å, respectively. The Brillouin zone was sampled by a $3 \times 3 \times 1$ k-point mesh, and the kinetic energy cutoff was set to 520 eV in the plane-wave expansion. To achieve high accuracy, the k-point value was increased to $5 \times 5 \times 1$ for energy band calculations.
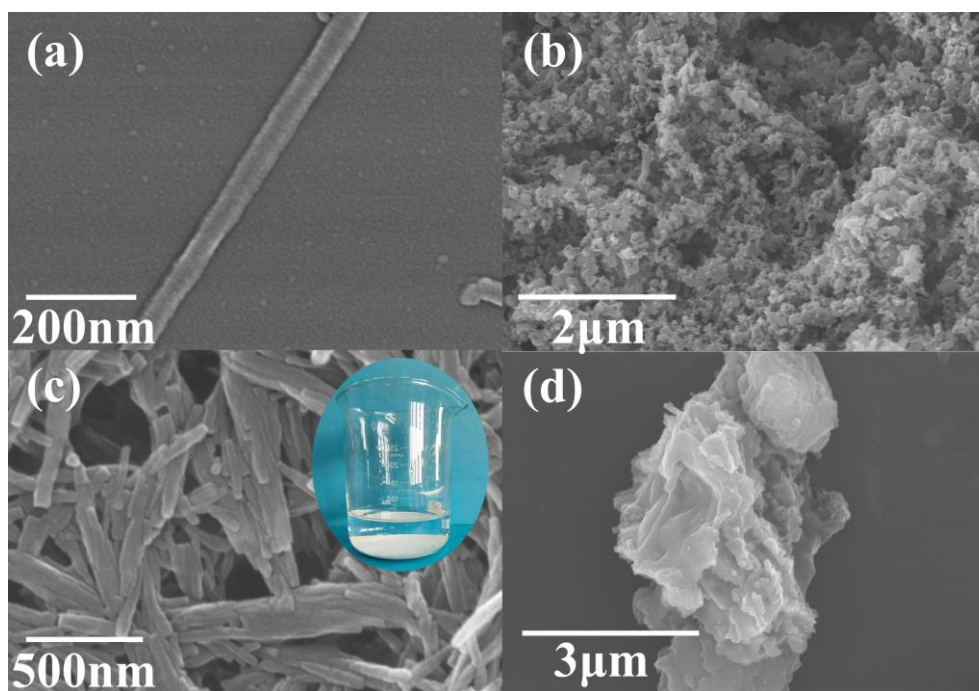
Fig.S1 SEM images of NP (a), TMCN (c), MP(c) and MCN (d).
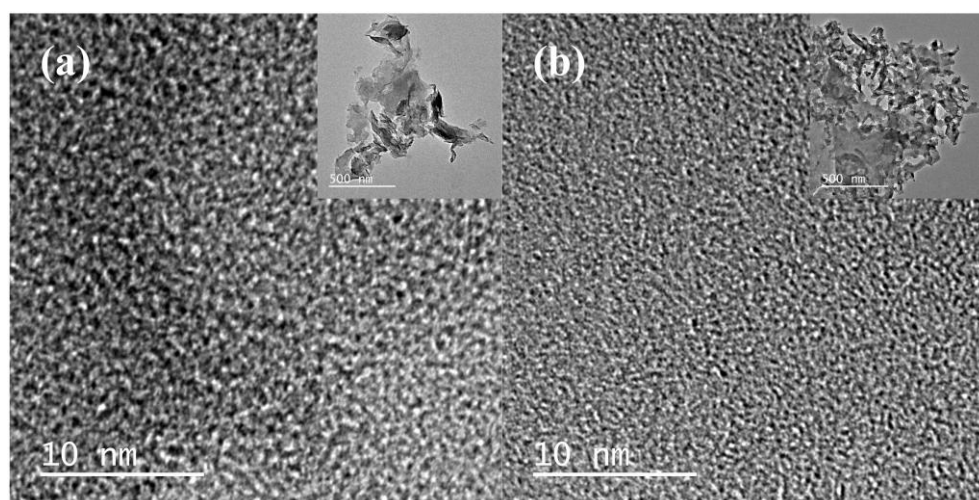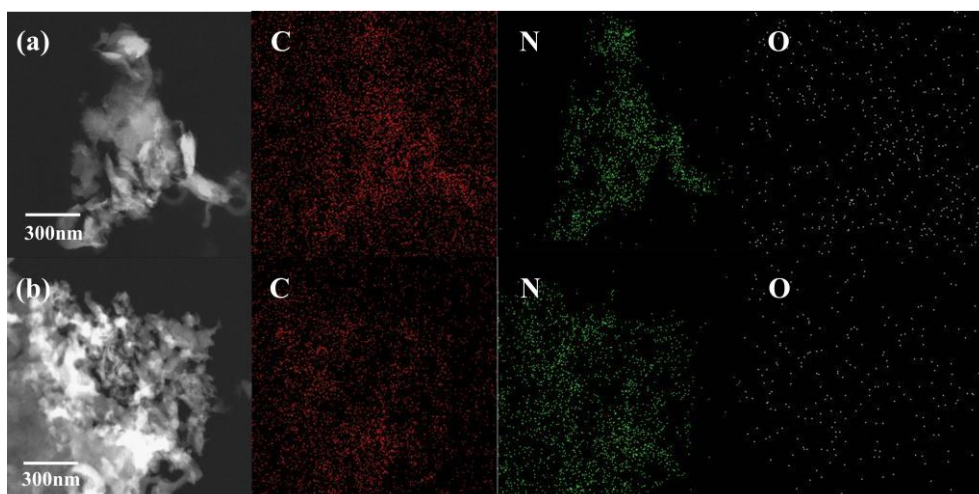
Fig. S2 HRTEM images of PCN (a) and TMCN (b).

Fig.S3 Mapping and EDS images of PCN (a) and TMCN (b).
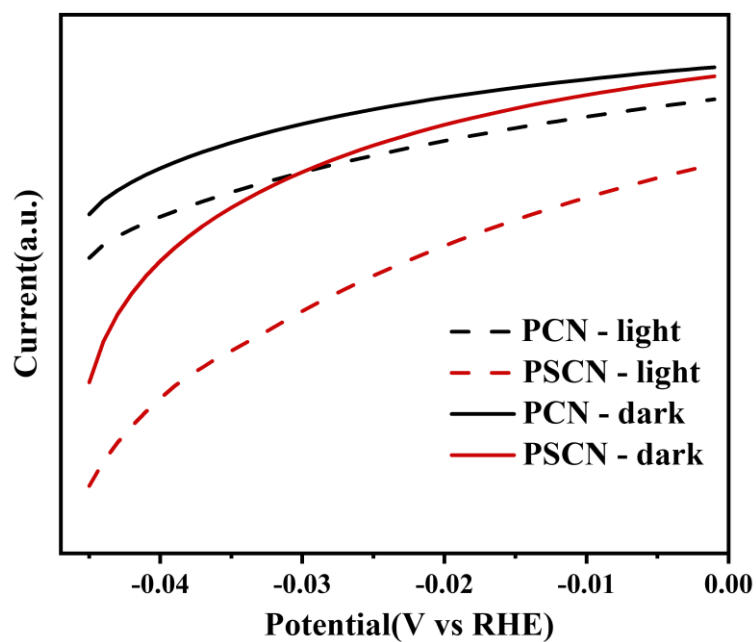
Fig. S4 Photo-responsive linear sweep voltammetry curves of PCN and TMCN.
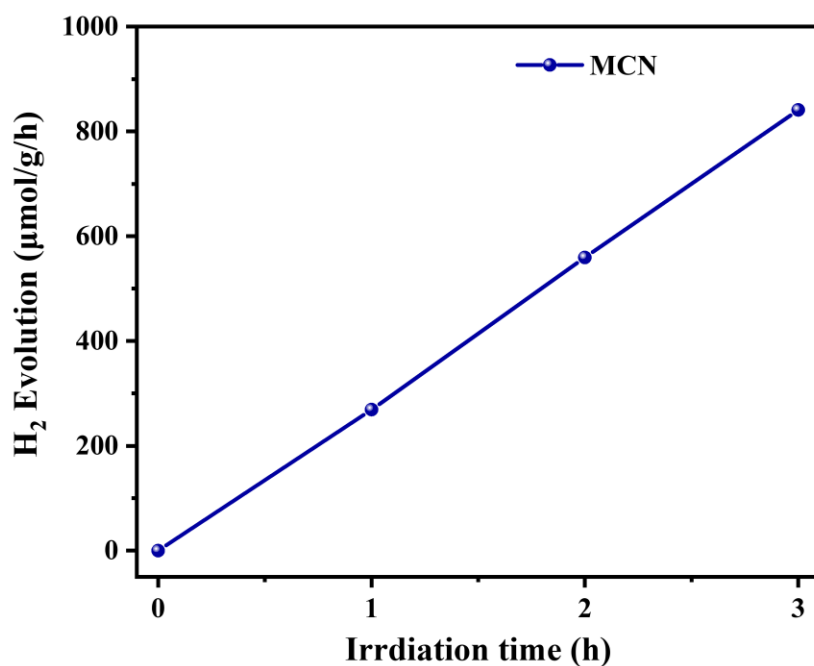
Fig. S5. Photocatalytic H_2 production rates of MCN.

Tab.S1 BET specific surface area and pore volume.

Samples	$S_{BET}(m^2/g)$	Pore volume(cm^3/g)
PCN	19.88	0.131
PSCN	58.50	0.188

Tab. S2 Atomic content of different elements in XPS spectrum.

Sample	C(at%)	N(at%)	O(at%)
PCN	41.40	52.77	5.83
PSCN	46.44	47.35	6.21

Tab. S3 Peak integration area of different carbon state in C1s spectrum.

Sample	C1	C2	C3	C4
PCN	22452.54	9064.2	113172.72	30497.69
PSCN	59177.57	8108.14	101824.39	37018.76

Tab. S4 Peak integration area of different carbon state in N1s spectrum.

Sample	N1	N2	N3
PCN	239395.18	61167.19	31345.33
PSCN	229698.67	54852.35	26186.42

Tab. S5 C/N atomic ratio in EA.

Sample	C/N
PCN	0.587
PSCN	0.588